Available online at www.sciencedirect.com

ScienceDirect

Chinese Journal of Aeronautics 20(2007) 385-393

Chinese Journal of Aeronautics

www.elsevier.com/locate/cja

The Full Flowpath Analysis of a Hypersonic Vehicle

Sun Shu*, Zhang Hongying, Cheng Keming, Wu Yizhao

College of Aerospace Engineering, Nanjing University of Aeronautics and Astronautics, Nanjing 210016, China

Received 9 November 2006; accepted 31 August 2007

Abstract

A numerical study has been carried out to investigate the full flow path and aerodynamic characteristics of a hypersonic vehicle at a 7.0 free stream Mach number. Results indicate that the inlet started and unstarted operations have remarkable effects on the flow pattern of the full flow path. When the inlet operates in a started mode, the transverse pressure gradient generated by the forebody alters the air captured characteristics and the entering flow quality of the inlet. Furthermore, the expansion process of the nozzle jet flow is obviously affected by the external flow field around the afterbody with the cross section shape transiting from a near rectangle at the exit of the nozzle to a near triangle at the tail of the vehicle. When the inlet operates in an unstarted mode, the aerodynamic instability can be observed in the full flow path of the vehicle. Due to the oscillation of the external compressed shock wave and nozzle jet flow, the aerodynamic characteristics of the vehicle vary periodically with the lift-drag ratio changing from 0.25 to 2.09. Finally, by comparing to the experimental data, the reliability of the CFD is verified.

Keywords: hypersonic vehicle; full flow path; inlet start; inlet unstart; unsteady; lift-drag ratio

1 Introduction

The insufficient net thrust obtained by hypersonic vehicles poses a formidable challenge to the design of various aerodynamic components in the propulsion system and the airframe. One promising technology that is capable of meeting the challenge is the airframe/propulsion integration. Since the 1960s, a lot of research studies have been dedicated to the integration of the propulsion system with the hypersonic airframe, including the integration of the inlet with the forebody, the integration of the nozzle with the afterbody, the optimization of the full flow path, the effects of the scramjet operating states on the aerodynamics of the airframe and so on[1-8]. Unfortunately, there are few papers that focus on the effects of the inlet started/unstarted condition on the flow pattern of the full flow path and the aerodynamic characteristics of the vehicle.

It is well known that hypersonic inlets should always operate in a started mode in the whole flight envelope. However, because of the immaturity of the current design methods and the uncertainties of the engine thrust regulations as well as the complex flight conditions, the unstarted condition of the inlet occurs inevitably during the development of hypersonic air-breathing propulsion system. According to Refs.[9-12], a prominent feature of unstarted hypersonic inlets is of an unsteady flow which can threaten the stable operation of the propulsion system and even lead to unsteady aerodynamic force and moment on the vehicle. Moreover, the unsteady aerodynamic characteristics will bring troubles to the flight control and the structure safety of the vehicle. Therefore, from both the academic and the practical point of view, it arises an urgent need for

*Corresponding author. Tel.: +86-25-84893476.
E-mail address: sunshu@nuaa.edu.cn
Foundation item: National Nature Science Foundation of China (5060601)

thorough investigation on the aerodynamic characteristics while the inlet is either in started or in unstarted mode. Recently, the influences of the inlet started/unstarted operations on the vehicle aerodynamic characteristics were experimentally studied by Ref.[13]. Some useful conclusions were drawn, but the complex phenomena still remain unclear because the pressure measurement adopted was of steady type and the FPS (frames per second) of the CCD camera was insufficient.

In order to gain a deep insight into the complex phenomena, the integrated flow field in Ref.[13] has been numerically studied in an unsteady manner in this paper. With the aid of CFD (short for computational fluid dynamics) technology, this paper acquires an intensive knowledge of the aerodynamic characteristics and the flow patterns of the full flow path while the inlet operates either in a started or in an unstarted state. Besides, the reliability of the CFD method is also verified by the experimental data in Ref. [13].

2 Methodology

2.1 Experimental setup

The internal and external configurations of the hypersonic vehicle(NX-1) are presented in Fig.1 and Fig2. The whole flow path consists of an inlet, an isolator, a combustor and a nozzle. The inlet is located at the aft part of the fuselage and the distance from the apex of the fuselage to the leading edge of the cowl is 253 mm. The shock-on-lip Mach number of the inlet is 7.0. The outside compression of the inlet is realized through three ramp surfaces with 5°, 6° and 3° turning angles respectively. The total area contraction ratio of the inlet is 7.0 with the internal one being 2.2. Downstream the throat of the inlet is followed by a constant cross-sectional duct with a length 4 times the throat height (H_0), which serves as the isolator. During the experiment, the throat height can be altered to obtain the inlet started or unstarted condition. The combustor has a small section of constant area succeeded by a duct with a 2° divergence angle. The injection holes and recessed cavities are not taken into account. Following the combustor, an expanding duct with divergence angles of 16° and 7° acts as a nozzle. Furthermore, a set of typical points are taken as follows: point *O*—the apex of the fuselage, point *A*—the entrance of the internal duct, point *B*—the exit of the isolator, point *C*—the entrance of the nozzle, and point *D*—the exit of the internal duct.

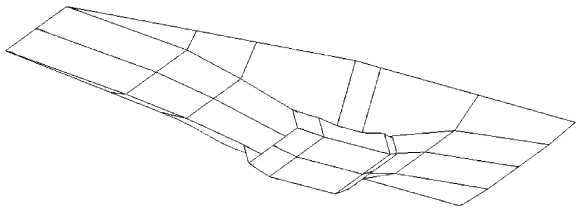

Fig.1 Configuration of the hypersonic vehicle.

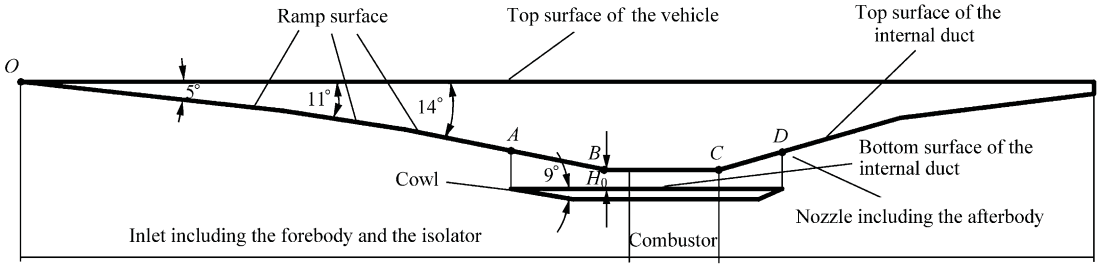

Fig.2 Sketch of the entire flow path.

The experiment is conducted in the hypersonic wind tunnel in Nanjing University of Aeronautics and Astronautics. The facility runs in a blown-down mode with a usable runtime greater than 4 s. The test section is in a 500 mm×500 mm rectangle form. Conditioned by the wind tunnel blockage, the test model is in the size of 140 mm (width)× 550 mm(length). In the experiment, should

be measured three parameters—the steady static pressures along the top surface of the flow path, the aerodynamic forces and the shadowgraph flow visualization. During the tests, the free stream Mach number is 7.0, the incident angle of the model 2° and the throat height of the inlet set to 5.0 mm or 7.0 mm. The inlet operates in a started mode when H_0 = 7.0 mm, and in a unstarted mode when H_0 = 5.0 mm. Further details of the experimental model can be found in Ref.[13].

2.2 Numerical approach

In order to eliminate the boundary effects on the CFD results, a large cubic flow domain 4 500 mm long, 1 000 mm wide and 1 000 mm high is chosen. In this study, a structured mesh has been used. The grid topology contains 55 blocks, which match completely each other and forms the complex flow domain with the total number of cells approximately 2 000 000. Fig.3 gives a close view of the surface grid, from which cells are found to cluster near the wall region and in the internal duct, which is caused by specifying the first cell height and the stretching ratio during the grid generation.

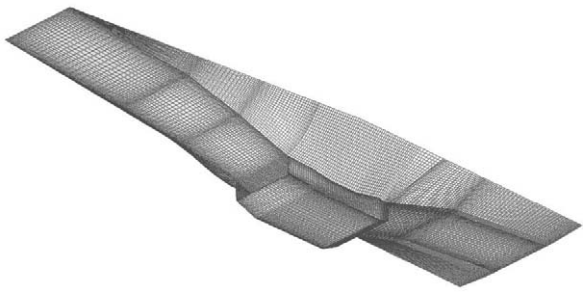

Fig.3 Surface grids of the hypersonic vehicle.

By utilizing a finite-volume spatial discretization, in which the state variables are stored at the cell center, the flow solver solves the compressible Reynolds-averaged time-dependent Navier-Stokes equations in three dimensions. To deal with the compressible effect on the flow, the governing equations are averaged by the Favre method. In computation, the inviscid convection flux scheme is Roe's method, and the MUSCL approach is used to obtain the characteristic variables on the control surfaces. The steady-state solution is obtained through the Gauss-Seidel relaxation. In computing unsteady flow, Runge-Kutta method is used and the calculations are started with a time step equal to 0.2 ms. The turbulence model used is the standard k-ε model and the standard wall functions are introduced to model the near-wall region flow. In the turbulence kinetic energy equation, effects of the compressibility are considered through modification of the turbulent fluctuating velocity term and the pressure dilatation term[14].

The convergence of each iteration is decided according to the residual histories of seven governing equations and the behavior of the aerodynamic forces of the vehicle. When the residual of each equation drops by four orders of magnitude with stable forces of the vehicle, the calculation is viewed as converged.

In numerical simulation, non-slip conditions are assumed for the walls of the vehicle and the temperature of the walls is set according to the experimental condition. Along the supersonic inflow boundaries, uniform conditions are used for the free stream. The pressure and other flow parameters at the outflow boundary are extrapolated from the interior domain.

3 Results and Discussion

In order to clarify the effects of inlet operating states on the flow pattern of the full flow path and the aerodynamic characteristics of the vehicle, numerical studies have been carried out in this paper.

3.1 Started operation

Fig.4 shows the contour plots of Mach number and static pressure of the symmetric plane where Ma_0 = 7.0, α = 2°, H_0 = 7.0 mm. In this figure, P_i/P_0 is the ratio of the local static pressure and the free stream static pressure. This figure demonstrates the flow process along the flow path that the flow firstly compressed by the inlet, rushes into the combustor and escapes into the atmosphere through the nozzle. It is noted that the presence of sharp and fairly stable external compression shocks without obvious

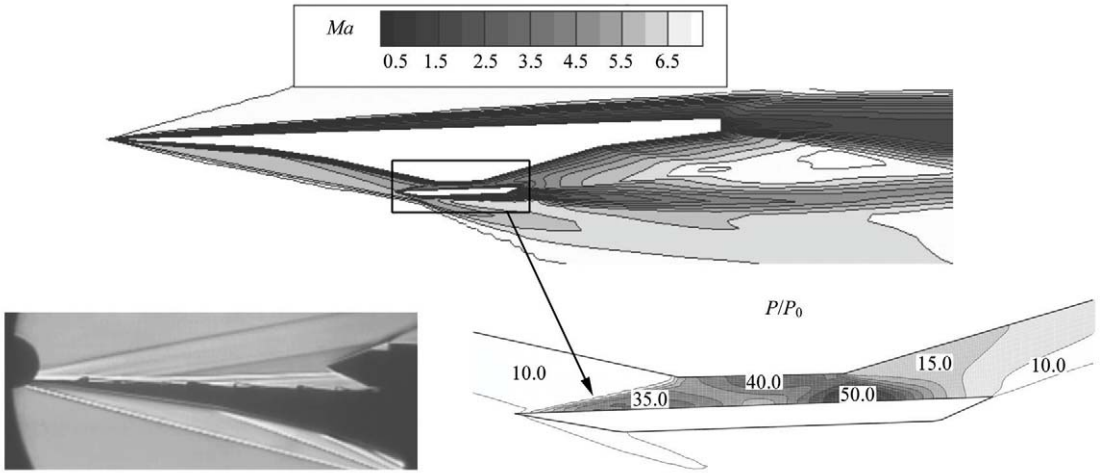

Fig.4 Flow pattern at the symmetric plane of the vehicle while the inlet is started.
(top—Mach number contours; bottom left—schlieren photo; bottom right—static pressure contours)

separation bubbles as well as the induced shocks suggests the inlet started. As shown in Fig.4, there is a complex shock system in the internal duct. The strong oblique shock wave produced by the local flow turning angle near the cowl impinges just upon the shoulder of the inlet. Thus, the reflected shock wave is weakened by the expansion wave near the shoulder, which results in a fairly uniform distribution of static pressure at the entrance of the isolator. The static pressure distribution along the ramp surface is presented in Fig.5, from which it can be seen that along the flow direction the static pressure gradually rises before the entrance of the inlet (point *A*). After that a pressure surge occurs and the maximum value is achieved between point *B* and point *C* due to the impingement shock wave caused by the cowl. After point *C* the static pressure gradually decreases as a result of the expansion process of the nozzle.

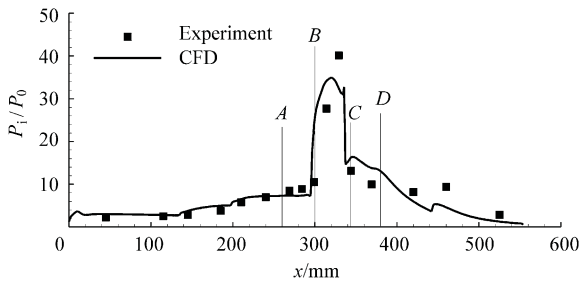

Fig.5 Static pressure distribution along the top surface of the flow path.

According to Fig.4 and Fig.5, it can be concluded that the flow pattern and the static pressure distribution obtained by CFD well accord with the experimental results. Table 1 shows the aerodynamic characteristics of the hypersonic vehicle. The computational results and the experimental results are also in good agreement with each other. The relative errors of the predicted drag coefficient, lift coefficient and lift-drag ratio are 8%, 13% and 6% respectively, which means acceptability of the reliability of the CFD method.

Table 1 Aerodynamic characteristics of NX-1 model while Ma_0=7.0, α=2°

	C_L	C_D	C_L/C_D
Computation	0.26	0.24	1.08
Experiment[12]	0.30	0.26	1.15

Fig.6 gives a clear picture of the flow structure of the forebody at Ma_0 = 7.0, α = 2° while the inlet is under the started condition. It can be found that an obvious pressure gradient along the spanwise direction of the forebody increases along the flow direction, which causes both negative and positive effects on the performance of the inlet. On the one hand, as the air flow goes downstream the pressure gradient

forces more and more pre-compressed air flow away from the inlet which results in low captured area ratio and extra drag penalty. On the other hand, as the pressure gradient also pushes part of the boundary layer flow away from the inlet, the entering flow quality and thus the performance and the operating stability of the inlet will be improved.

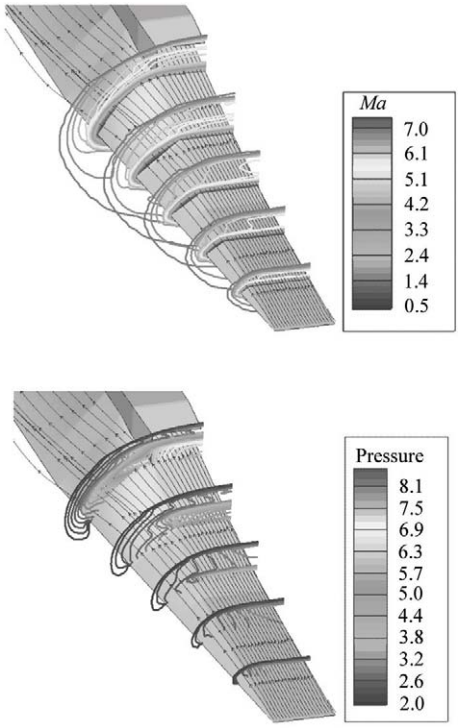

Fig.6 Flow structure of the forebody while the inlet operate in a started mode.

The flow structure of the afterbody at Ma_0 = 7.0, α = 2° is demonstrated in Fig.7, in which the streamlines are emitted from the out surface of the jet flow. Following the internal expansion, the jet flow continues to expand under the surface constraint of the nozzle ramp and the cross-sectional size of the jet flow increases gradually both in height and in width. Furthermore, as the flow goes downstream, the Mach number of the core flow increases gradually and the intensity of the shear layer between the jet flow and the external flow becomes weaker as an accumulative result of the viscosity effects. Moreover, the cross-sectional shape of the jet flow changes from a near rectangle at the exit of the nozzle into a near triangle at the tail of the vehicle due to the strong interactions of the outflow with the jet flow.

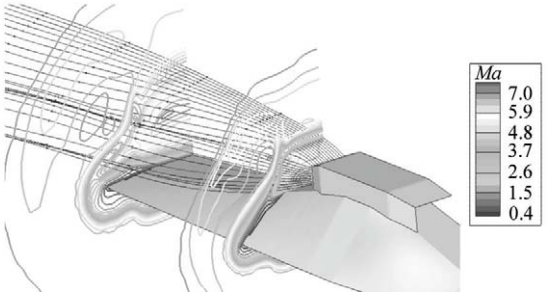

Fig.7 Flow structure of the afterbody while the inlet operates in a started mode.

3.2 Unstarted operation

The experimental results of Ref.[13] indicate that the unsteady characteristics of the flow pattern is prominent when the inlet is in a unstarted state at Ma_0 = 7.0, α = 2°, H_0 = 5 mm. However, the adopted experimental measurements prevent a thorough knowledge of the influences of a unstarted inlet on the aerodynamic performances of the hypersonic vehicle. Thus the unsteady calculations are relied on to make things much clearer. Fig.8 presents the time histories of aerodynamic characteristics of the hypersonic vehicle. It can be seen that when the inlet is unstarted, the instantaneous aerodynamic forces fluctuate periodically and substantially. In a typical cycle, the time averaged lift-drag ratio is 0.85, which well matches the experimental results in Ref.[13], but the instantaneous lift-drag ratio peaks at 2.09 and bottoms out at 0.25.

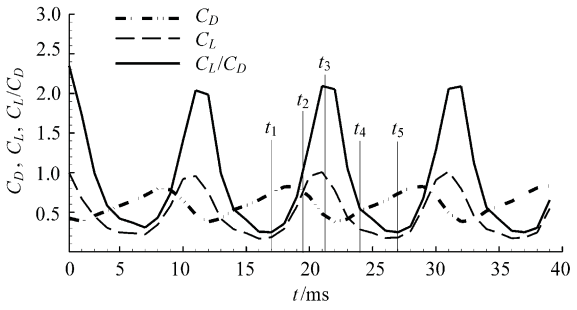

Fig.8 Time histories of the aerodynamic characteristics of the hypersonic vehicle while the inlet is unstarted.

In Fig.9, the flow patterns of the full flow path at five different temporal points (t_1, t_2, t_3, t_4, t_5) are shown on a symmetric plane to explain the trends of the aerodynamic forces. From the figure, it can be found that the flow pattern of the full flow path is

unsteady with a shock system at the entrance oscillating along the flow direction and the jet flow from the nozzle alternating in expanding and shrinking, which results in fluctuation of the aerodynamic forces along with the time. The corresponding instantaneous static pressure distributions on the top surface of the flow path are shown in Fig.10. With Fig.9 and Fig.10, the instantaneous flow patterns and the corresponding aerodynamic characteristics can be analyzed as follows.

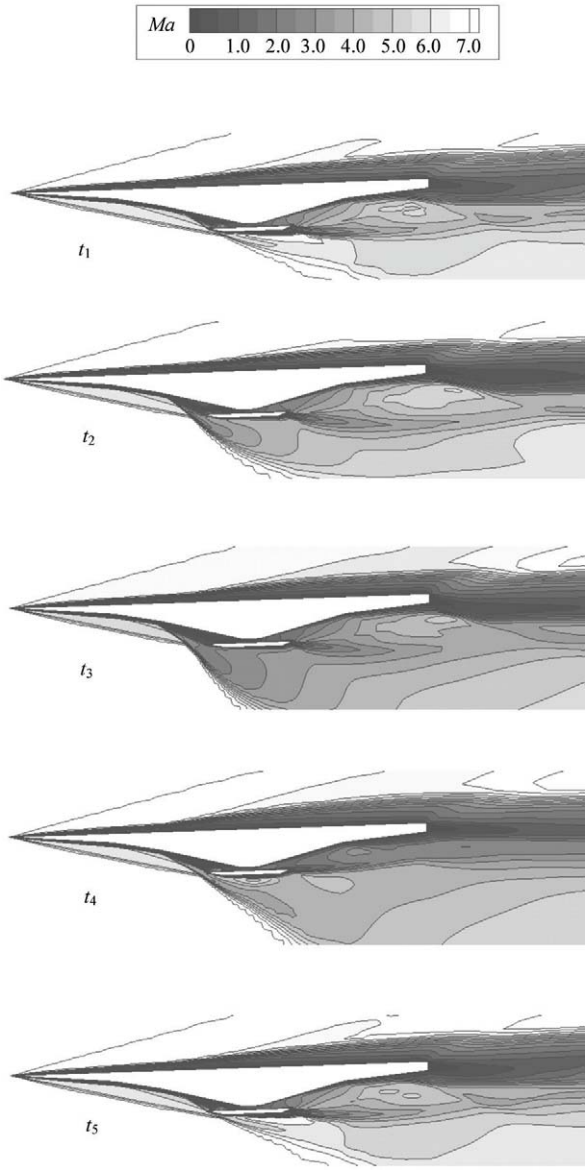

Fig.9 Instantaneous contour plots of Mach number at five different temporal points (t_1, t_2, t_3, t_4, t_5) when the inlet is unstarted.

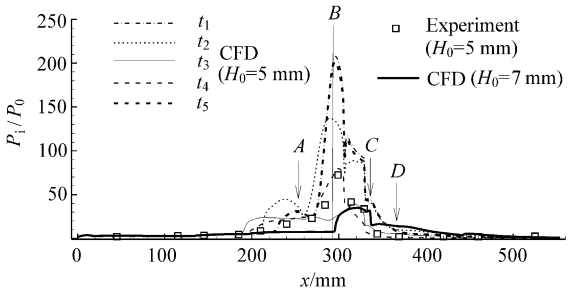

Fig.10 Instantaneous static pressure distributions of the top surface at five different temporal points (t_1, t_2, t_3, t_4, t_5) when the inlet is unstarted.

(1) At the temporal point of t_1, the shock-on-lip condition is met without noticeable flow spillage from the cowl. Because the mass flow captured by the inlet exceeds the maximum flow capacity of the duct with a throat 5 mm high, the duct is choked at this moment. Therefore, it can be noted in Fig.10 that in the contract part of the inlet, P_i/P_0 peaks at 200 which is five times the value when H_0 is 7 mm. The ultra-high internal static pressure forms an asymmetry shock train in the contract part of the inlet and induces a strong oblique shock at the entrance (Fig.9) because of the intensive shock/boundary layer interactions, which substantially increases the static pressure of the forebody and the contract part as compared with the inlet started condition. The increased static pressure of the forebody and the contract part makes the drag coefficient reach 0.79 which approximates the maximum value in a cycle. Despite the substantial static pressure increase of the forebody and the contract part, the lift coefficient at this moment bottoms out at 0.23 in a cycle and is almost equal to the value of the inlet started operation. This is attributable to the balance of the high pressure on top surface and bottom surface of the internal duct. The decreased afterbody surface pressure also prevents the increase of the lift coefficient. But it can be concluded that the pitching moment of the vehicle is much different from that of the inlet started operation.

(2) At the temporal point of t_2, due to the high pressure near the throat, the separation bubble near the entrance is enlarged and pushed toward the leading edge of the forebody. Thus the external

compression shock system is forced to move away from the cowl lip, which results in a large supersonic spillage and alleviates the mass flow accumulation in the duct. At this moment the peak value of P_i/P_0 is decreased to 150. However, as compared with the temporal point of t_1, the drag coefficient of t_2 still maintains a high value because the high pressure region of the forebody is enlarged while the separation bubble moves upstream. On the other hand, the large region of forebody bottom surface with high static pressure increases the lift coefficient of the vehicle substantially. In consequence, the lift-drag ratio at this moment is much higher than that of t_1.

(3) At the temporal point of t_3, the separation bubble and the external compression shock system move to the farthest position away from the entrance. In Fig.9, it can be noted that the separation bubble occupies almost the entire height of the entrance. Thus the flow captured by the inlet is substantially reduced. In Fig.10, a plateau region of static pressure appears in the contract part of the inlet as a result of the large seperation bubble. The static pressure level of the plateau region approximates the pressure value just behind the induced oblique shock. At this moment, both the peak static pressure of the internal duct and the drag coefficient of the vehicle decrease to the lowest level in a cycle, while the lift coefficient increases to the highest due to the enlargement of the high pressure region near the forebody. Thus, at the temporal point of t_3 the lift-drag ratio of the vehicle reaches the highest level in a cycle.

(4) In the temporal region between t_3 and t_5, due to the low pressure region of the contract part formed at t_3, the separation bubble near the forebody declines and moves toward to the entrance of the duct. Therefore, the external compression shock system begins to move back and the mass flow captured by the inlet increases gradually until the shock-on-lip system is maintained again at the temporal point of t_5. During this process, the static pressure of the contract part of the inlet rises continuously due to the increased mass flow. When the captured mass flow exceeds the maximum flow capacity of the duct at t_5, the internal duct is choked again and the external shock system begins moving upstream. The instantaneous static pressure distribution at this moment almost coincides with that of t_1 meaning the start of a new cycle.

Fig.11 presents the flow patterns of the forebody at different temporal points from t_1 to t_3 while $Ma_0 = 7.0$, $\alpha = 2^\circ$, $H_0 = 5$ mm. It can be seen that the separation bubble near the entrance is obvious at these temporal points. While the temporal point changes from t_1 to t_3, the height of the separation bubble increases gradually while the width remains almost unchanged. Also it is notable that most part of the forebody flow field is substantially influenced by the inlet unstarted phenomenon, which evidently changes the aerodynamic loads of the vehicle.

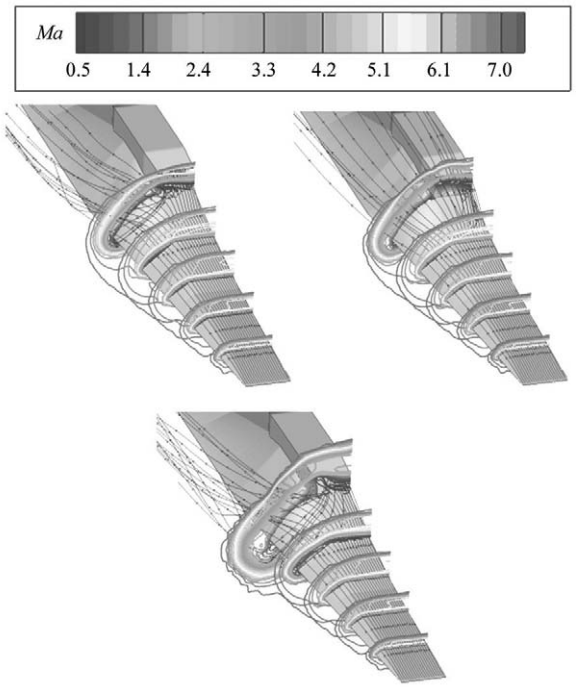

Fig.11 Instantaneous flow patterns of the forebody at typical temporal points from t_1 to t_3 while the inlet is unstarted.

The flow patterns of the afterbody at different temporal points from t_1 to t_3 are demonstrated in Fig.12. It can be seen that, though the average static pressure at the exit of internal duct under the inlet unstarted condition is lower than that under the inlet started condition, the jet flow from the nozzle at t_2

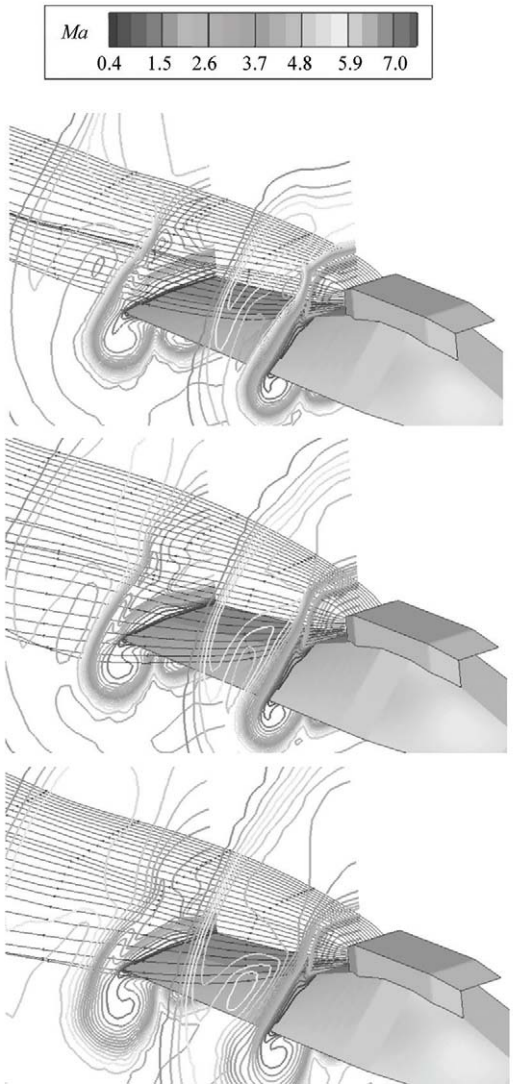

Fig.12 Instantaneous flow patterns of the afterbody at typical temporal points of t_1 to t_3 while the inlet is unstarted.

and t_3 expands more significantly. According to a detailed analysis of the CFD results, it is found that there exist differences between the inlet started condition and unstarted condition in the respect of interaction of the jet flow of the nozzle with the external flow around the afterbody. In fact, under the inlet started condition or at the temporal point of t1 while the inlet is unstarted, the Mach number of the external flow around the afterbody is high and the extrusion effect of the external flow on the jet flow is strong. But at the temporal points of t_2 and t_3 while the inlet is in a unstarted state, the separation bubble and the induced strong shock wave in front of duct exert significant effects on the flow field surrounding the engine and substantially reduces the instantaneous Mach number of the external flow field. As a result, the jet flow is less constrained by the external flow and expands more freely.

4 Conclusions

A numerical study has been carried out to study the flow field of the entire flow path and the aerodynamic characteristics of a hypersonic vehicle at a 7.0 free stream Mach number. The emphasis of the analysis is placed on the effects of the inlet operating conditions. Results indicate that the inlet started and unstarted operations have remarkable impacts on the flow pattern of the full flow path. When the inlet operates in a started state, the transverse pres-sure gradient generated by the forebody alters the air-capture characteristics and the entering flow quality of the inlet. The expansion of the nozzle jet flow is obviously affected by the external flow around the afterbody with a continuous cross sectional shape changing along the flow direction. When the inlet operates in a unstarted state, substantial aerodynamic instabilities can be observed in the entire flow path of the vehicle. Due to the oscillations of the external compression shock system and the nozzle jet flow, the aerodynamic characteristics of the vehicle vary periodically with the lift-drag ratio changing from 0.25 to 2.09.

References

[1] Akihsa D, Masuya G. Effects of airframe integrated configuration on scramjet inlet performance. AIAA 2000-0619, 2000.

[2] Liu Jia, Yao Wenxiu, Lei Maifang, et al. Forebody compressibility research of hypersonic vehicle. Applied Mathematics and Mechanics 2004; 25(1): 85-92. [in Chinese]

[3] Tan Huijun, Guo Rongwei. Wind tunnel tests of hypersonic inlets for ramjet modules of ramjet-scramjet combined engine. Acta Aeronautica et Astronautica Sinica 2007; 28(4): 783-790. [in Chinese]

[4] Kobyashi H, Sato T, Tanataugu N. Optimization of airbreathing propulsion system for the TSTO space-plane. AIAA 2001-1912, 2001.

[5] Tsuchiya T, Mori T, Maita M. An integrated optimization for conceptual designs of airbreathing launch TSTO vehicle. AIAA

2001-1902, 2001.

[6] Ryan P, Mark S, Lewis J. Critical design issues for air-breathing hypersonic waverider missiles. Journal of Spacecrafts and Rockets 2001; 38(4): 510-519.

[7] He Yuanyuan. Numerical study of airframe/propulsion integrative hypersonic vehicle. PhD thesis, China aerodynamics research and development center; 2004. [in Chinese]

[8] Tan Huijun, Guo Rongwei. Characteristics of shock train in two dimensional bends with constant area. Acta Aeronautica et Astronautica Sinica 2006; 27(6): 1039-1045. [in Chinese]

[9] von Eggers Lael, Darryll R, Pines J. Integrated propulsion effects on dynamic stability and control of hypersonic watersides. AIAA 2000-3826, 2000.

[10] Scott D H. Wind-tunnel blockage and actuation systems test of a two-dimensional scramjet inlet unstart model at Mach 6. NASA-TM-109152, 1994.

[11] Van Wie D M, Kwok F T, Walsh R F. Starting characteristics of supersonic inlets. AIAA-96-2914, 1996.

[12] Tan H J, Guo R W. Experimental study of the unstable-unstarted condition of a hypersonic inlet at Mach 6. AIAA Journal of Propulsion and Power 2007; 23(4): 783-788.

[13] Zhang Hongying, Sun Shu, Cheng Keming, et al. Experimental investigation of inlet start/unstart influences on the aerodynamic characteristic of a hypersonic vehicle. Journal of Astronautics, in press. [in Chinese]

[14] Krishnamurty V S, Clutter J K, Shyy W. Study of two-equation based modelling for compressible turbulent flows. AIAA 96-0518, 1996.

Biography:

Sun Shu Born in 1979, she received B.S. and Ph.D. from Nanjing University of Aeronautics and Astronautics in 2001 and 2006 respectively, Now she is a post-doctoral researcher in this university. Her main research interest lies in inlet and airframe/propulsion integration.

E-mail: sunshu@nuaa.edu.cn